



UDC 621.762.34

<https://doi.org/10.17073/1997-308X-2025-2-5-14>

Research article

Научная статья



Comparison of properties of hard magnetic isotropic powder-processed Fe–Cr–Co alloys doped with titanium and titanium hydride

A. S. Ustyukhin¹ , V. A. Zelensky¹, I. M. Milyaev¹,D. Yu. Kovalev², V. S. Shustov¹, M. I. Alymov^{1,2}¹A.A. Baikov Institute of Metallurgy and Materials Science of the Russian Academy of Sciences

49 Leninskiy Prosp., Moscow 119334, Russia

²Merzhanov Institute of Structural Macrokinetics and Materials Science of the Russian Academy of Sciences

8 Academician Osipyan Str., Chernogolovka, Moscow Region 142432, Russia

 fcneo@yandex.ru

Abstract. This study presents a comparative investigation of the density, phase composition, magnetic, and mechanical properties of isotropic powder metallurgy alloys Fe–28Cr–15Co and Fe–32Cr–22Co doped with 2 wt. % titanium introduced either as conventional titanium powder (PTS-1 grade) or as titanium hydride powder. The sample fabrication process included powder blend preparation, compaction, vacuum sintering, quenching, and heat treatment aimed at developing magnetic properties. The use of titanium hydride powder resulted in an increase in residual porosity from 2 to 4 %. A significant difference in the phase composition of the alloys after sintering was observed: the structure of the Fe–28Cr–15Co–2Ti alloy consisted of a BCC α -phase solid solution and tetragonal σ -phase inclusions, while Fe–32Cr–22Co–2Ti exhibited a σ -phase solid solution matrix with FCC γ -phase inclusions. After heat treatment, all alloys developed a BCC α -phase solid solution structure. In the samples containing titanium hydride, minor traces of an impurity phase – most likely a hydride of a titanium–chromium intermetallic compound – were also detected. Samples prepared using PTS-1 titanium powder exhibited higher residual induction values (B_r , up to 0.84 and 0.82 T for Fe–28Cr–15Co–2Ti and Fe–32Cr–22Co–2Ti, respectively) compared to those containing titanium hydride (up to 0.80 and 0.79 T, respectively), which is attributed to differences in residual porosity. On the other hand, samples with titanium hydride powder showed higher coercivity values (H_c , up to 41.1 and 57.2 kA/m for Fe–28Cr–15Co–2Ti and Fe–32Cr–22Co–2Ti, respectively) compared to those with titanium powder (up to 38.4 and 49.2 kA/m, respectively). The maximum energy product $((BH)_{max})$ reached 11.0–11.5 kJ/m³ for Fe–28Cr–15Co–2Ti and 14.0–14.5 kJ/m³ for Fe–32Cr–22Co–2Ti, with virtually no dependence on the titanium source. The compression stress–strain curves for alloys with different titanium sources were nearly identical. Alloys of the Fe–32Cr–22Co–2Ti composition exhibited higher yield strength values ($\sigma_{0.2}$ = 1200–1400 MPa) compared to Fe–28Cr–15Co–2Ti alloys ($\sigma_{0.2}$ = 1000 MPa). All materials studied in this work demonstrated ductility.

Keywords: powder metallurgy, heat treatment, Fe–Cr–Co alloys, doping, porosity, magnetic properties, mechanical properties

Acknowledgements: This work was financially supported by the Russian Science Foundation, Project No. 24-29-00323.

For citation: Ustyukhin A.S., Zelensky V.A., Milyaev I.M., Kovalev D.Yu., Shustov V.S., Alymov M.I. Comparison of properties of hard magnetic isotropic powder-processed Fe–Cr–Co alloys doped with titanium and titanium hydride. *Powder Metallurgy and Functional Coatings*. 2025;19(2):5–14. <https://doi.org/10.17073/1997-308X-2025-2-5-14>

Сравнение характеристик магнитотвердых порошковых изотропных Fe–Cr–Co-сплавов, легированных титаном и гидридом титана

А. С. Устюхин¹, В. А. Зеленский¹, И. М. Миляев¹,
Д. Ю. Ковалев², В. С. Шустов¹, М. И. Алымов^{1, 2}

¹ Институт металлургии и материаловедения им. А.А. Байкова Российской академии наук
Россия, 119334, г. Москва, Ленинский пр-т, 49

² Институт структурной макрокинетики и проблем материаловедения
им. А.Г. Мержанова Российской академии наук
Россия, 142432, Московская обл., г. Черноголовка, ул. Акад. Осипьяна, 8

✉ fcbneo@yandex.ru

Аннотация. В работе проведено сравнительное исследование плотности, фазового состава, магнитных и механических свойств изотропных порошковых сплавов Fe–28Cr–15Co и Fe–32Cr–22Co, легированных 2 мас. % титана в виде обычного порошка титана ПТС-1 и порошка гидрида титана. Процесс получения образцов состоял из приготовления исходной смеси порошков, прессования, спекания в вакууме, закалки и термической обработки для формирования магнитных свойств. Использование порошка гидрида титана привело к повышению остаточной пористости образцов с 2 до 4 %. Было отмечено существенное отличие фазового состава сплавов после спекания: структура образца Fe–28Cr–15Co–2Ti состояла из твердого раствора ОЦК α -фазы и включений тетрагональной σ -фазы, а Fe–32Cr–22Co–2Ti – из твердого раствора σ -фазы и включений ГЦК γ -фазы. После термической обработки структура всех сплавов представляла собой твердый раствор ОЦК α -фазы. В образцах с гидридом титана были также обнаружены малые следы примесной фазы, которая, вероятнее всего, является гидридом интерметаллического соединения титана и хрома. Образцы, в которых использовался порошок титана ПТС-1, имели более высокие значения остаточной индукции (B_r до 0,84 и 0,82 Тл у сплавов Fe–28Cr–15Co–2Ti и Fe–32Cr–22Co–2Ti соответственно) по сравнению с образцами, содержащими гидрид титана (до 0,8 и 0,79 Тл соответственно), что связано с разницей в остаточной пористости. С другой стороны, образцы с порошком гидрида титана имели более высокие показатели коэрцитивной силы (H_c до 41,1 и 57,2 кА/м у сплавов Fe–28Cr–15Co–2Ti и Fe–32Cr–22Co–2Ti соответственно) по сравнению с образцами, содержащими порошок титана (до 38,4 и 49,2 кА/м соответственно). Наиболее высокие значения максимального энергетического произведения $(BH)_{max}$ составили 11,0–11,5 кДж/м³ у сплавов Fe–28Cr–15Co–2Ti и 14,0–14,5 кДж/м³ у Fe–32Cr–22Co–2Ti и практически не зависели от типа введенного титана. Кривые деформирования при сжатии сплавов с разными источниками титана были практически идентичны. Образцы состава Fe–32Cr–22Co–2Ti имели более высокие значения предела текучести ($\sigma_{0,2} = 1200 \div 1400$ МПа) по сравнению со сплавами Fe–28Cr–15Co–2Ti ($\sigma_{0,2} = 1000$ МПа). Все исследованные в работе материалы оказались пластичными.

Ключевые слова: порошковая металлургия, термическая обработка, Fe–Cr–Co-сплавы, легирование, пористость, магнитные свойства, механические свойства

Благодарности: Работа выполнена при финансовой поддержке РНФ, проект № 24-29-00323.

Для цитирования: Устюхин А.С., Зеленский В.А., Миляев И.М., Ковалев Д.Ю., Шустов В.С., Алымов М.И. Сравнение характеристик магнитотвердых порошковых изотропных Fe–Cr–Co-сплавов, легированных титаном и гидридом титана. *Известия вузов. Порошковая металлургия и функциональные покрытия.* 2025;19(2):5–14.
<https://doi.org/10.17073/1997-308X-2025-2-5-14>

Introduction

Hard magnetic alloys are among the most important materials in modern manufacturing, and the demand for them continues to grow. However, the majority of such alloys have high production costs due to the expensive components they contain, such as rare-earth metals and cobalt. Fe–Cr–Co-based hard magnetic materials contain less cobalt and therefore represent a more economical alternative. These materials exhibit a sufficient level of magnetic properties, although they are inferior in this

regard to many other magnetic systems [1–3]. The main advantages of Fe–Cr–Co alloys include the highest ductility among all hard magnetic materials, high strength and corrosion resistance, thermal stability, and a wide operating temperature range [4–8]. Recent studies on Fe–Cr–Co alloys have increasingly employed various approaches, primarily based on powder metallurgy and additive manufacturing technologies [9–18]. There is also ongoing research into the characteristics of magnetic films based on these alloys, which are used in non-contact sensors for various devices [19; 20].

In Fe–Cr–Co hard magnetic alloys, spinodal decomposition occurs at temperatures around 650 °C, during which the body-centered cubic (BCC) α -phase separates into two BCC phases, α_1 and α_2 , differing in chemical composition. During heat treatment – specifically, slow cooling from ~650 °C – ferromagnetic α_1 -phase particles become uniformly distributed in the weakly magnetic α_2 -phase matrix, leading to the development of magnetic properties in the alloy [21–23]. The parameters of the heat treatment process require careful control, as prolonged annealing or slow cooling can result in the formation of an equilibrium nonmagnetic σ -phase with a tetragonal crystal structure [24].

The properties of Fe–Cr–Co alloys can be modified by introducing various alloying elements, such as Mo, Si, W, Ti, and others [25–28]. When using powder metallurgy methods, a number of additional factors must be considered for alloying additives, including their solubility in the solid solution of the base elements (Fe, Cr, and Co), their reactivity with oxygen from the air trapped in the pores of the green compacts, and the characteristics of the initial powders. As shown in our experiments, the properties of the resulting material depend on the form in which the doping elements are introduced into the initial powder mixture [29].

The present study focuses on a comparative investigation of the properties of isotropic powder metallurgy Fe–Cr–Co alloys doped with titanium introduced either as conventional titanium powder or as titanium hydride powder. Dehydrogenation of the latter begins at approximately 450 °C and is expected to occur during the heating stage and throughout the sintering process. The study was conducted on alloys with the following compositions (wt. %): Fe–28Cr–15Co and Fe–32Cr–22Co, representing medium and high cobalt contents, respectively. Each alloy was doped with 2 wt. % of the above-mentioned titanium powders. The density, phase composition, as well as the magnetic and mechanical properties of the resulting compositions were investigated.

Materials and methods

To prepare the initial powder blends for the Fe–Cr–Co alloys, elemental powders of iron (carbonyl iron, grade VS), chromium (grade PX-1M), and cobalt (grade PK-1) with particle sizes of $d < 25 \mu\text{m}$ were used. Titanium was introduced into the system in two forms: titanium powder (PTS-1 grade) with $d < 45 \mu\text{m}$, and titanium hydride powder obtained by hydrogenating titanium sponge (grade TG-100, GOST 17746–96), followed by milling to a powder with $d < 45 \mu\text{m}$. Depending on the alloy composition (Fe–28Cr–15Co and Fe–32Cr–22Co) and the titanium source, the mate-

rials are hereafter designated as Kh28K15T_H, Kh28K15T_P, Kh32K22T_H, and Kh32K22T_P, where the subscripts “H” and “P” indicate titanium hydride and titanium powder (PTS-1), respectively. The powders were mixed in a Turbula shaker mixer C2.0 (Russia) for 300 min. For every 100 g of powder blend, 200 g of 3 mm diameter steel balls were added to the mixing container. Cylindrical green compacts weighing 20 g and measuring 13.6 mm in diameter were formed using a Knuth HP15 hydraulic press (Germany) under a compaction pressure of 600 MPa. The compacts were then sintered in a ShSV-1.2.5/25I1 electric vacuum furnace (Russia) at a pressure below 10^{-2} Pa and a temperature of 1350 °C, with an isothermal hold time of 2.5 h. After sintering, the density of the samples was determined using the hydrostatic weighing method in distilled water.

Subsequently, the alloys were heated to 1300 °C and quenched in water. After quenching, heat treatment was performed in a tube furnace to achieve a high-coercivity state. For each sample, four heat treatment modes were tested by varying the initial temperature (t_1). The heat treatment process consisted of the following three stages:

- 1) isothermal holding for 40 min at $t_1 = 630 \div 655$ °C;
- 2) cooling by 60 °C from t_1 at a rate of $v_1 = 20$ °C/h;
- 3) cooling to 500 °C at a rate of $v_2 = 8$ °C/h.

No external magnetic field was applied during the heat treatment.

Microscopic investigations were conducted using a TESCAN VEGA3 scanning electron microscope (Czech Republic). Elemental composition was analyzed by energy-dispersive spectroscopy (EDS) with an X-Act microanalyzer (Oxford Instruments, UK). The phase composition of the samples was examined by X-ray diffraction (XRD) using a Difrey-401 diffractometer (Russia) with CrK_α radiation, in the 2θ range of 35 to 125°. Magnetic hysteresis properties were measured using a Permagraph L hysteresisgraph (Magnet-Physik, Germany). Compression tests were performed using an Instron 3382 testing machine (Instron, USA) at a loading rate of 1 mm/min. For testing, cylindrical samples were machined to a diameter of 7 mm and a height of 15 mm.

Results and discussion

Table 1 presents the density values (ρ) of the titanium-doped powder Fe–Cr–Co alloys after sintering, as measured by the hydrostatic weighing method. The theoretical density (ρ_t) was calculated based on the principle of additivity: the density of each alloy component was multiplied by its respective weight fraction, and the results were summed. Based on these

Table 1. Density measurements of the investigated alloys with different titanium sources after sintering

Таблица 1. Результаты измерения плотности исследуемых сплавов с разными источниками титана после спекания

Alloy	ρ , g/cm ³	ρ_t , g/cm ³	ρ_{rel} , %
Kh28K15T_H	7.45–7.48	7.77	95.9–96.3
Kh28K15T_P	7.59–7.68	7.77	97.7–98.8
Kh32K22T_H	7.53–7.59	7.81	96.4–97.1
Kh32K22T_P	7.66–7.74	7.81	98.1–99.1

data, the relative density (ρ_{rel}) and residual porosity of the sintered samples were determined.

The results revealed noticeable differences in the density of the samples depending on whether titanium powder or titanium hydride powder was used for doping. According to the measured ρ values, the use of titanium hydride powder as the titanium source leads to an increase in porosity – up to 3.0–3.5 % for Kh32K22T_H samples and up to 4 % for Kh28K15T_H.

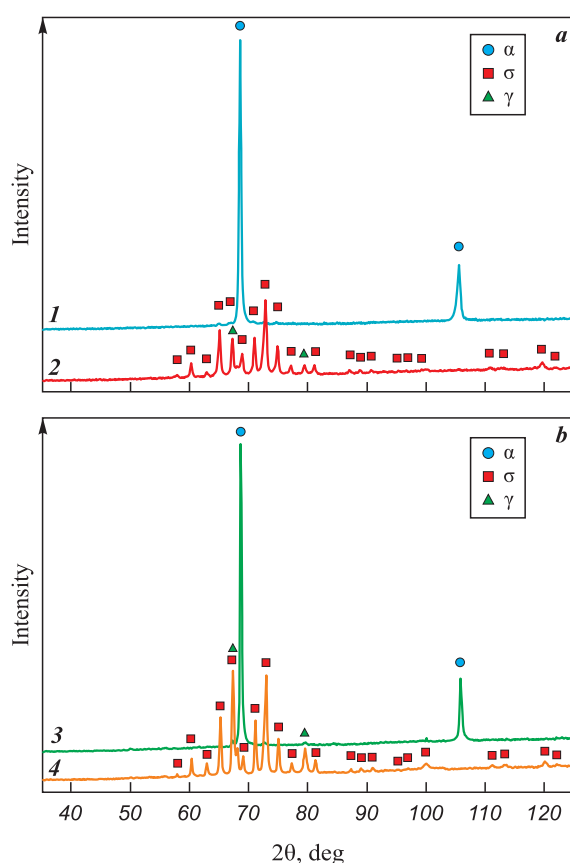


Fig. 1. X-ray diffraction patterns of Fe–Cr–Co alloys doped with titanium powder (a) and titanium hydride (b)

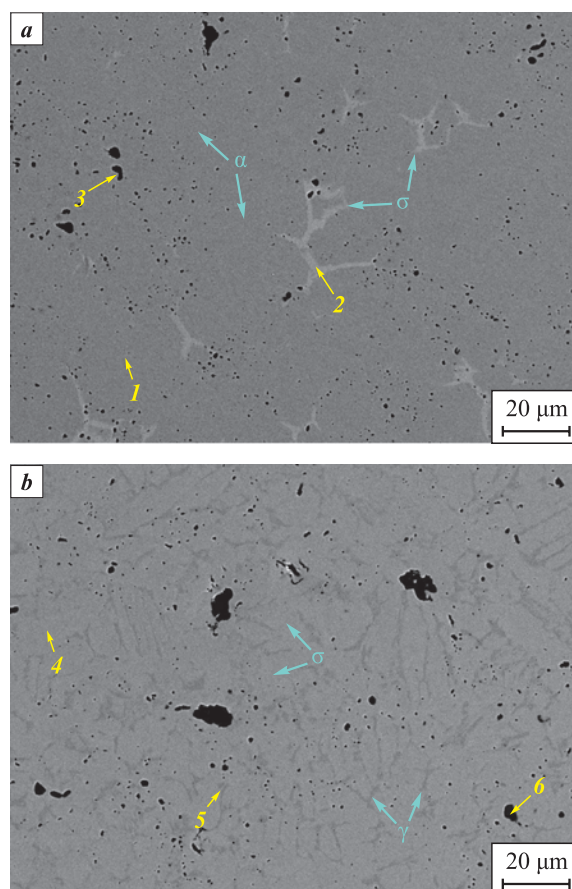
1 – Kh28K15T_H, 2 – Kh32K22T_H, 3 – Kh28K15T_P, 4 – Kh32K22T_P

Рис. 1. Дифрактограммы Fe–Cr–Co-сплавов, легированных порошком титана (a) и гидридом титана (b)

1 – X28K15T_Г, 2 – X32K22T_Г, 3 – X28K15T_П, 4 – X32K22T_П

According to our previous studies on powder Fe–Cr–Co alloys under the same sintering conditions, the relative density ρ_{rel} typically reaches approximately 98 % [11]. When titanium powder is used, the alloys exhibit a relative density of approximately 98–99%.

Fig. 1 shows the results of phase composition analysis of the alloys doped with PTS-1 titanium powder and titanium hydride immediately after sintering. Fig. 2 presents, as an example, microstructure images of the Kh28K15T_P and Kh32K22T_P alloys, along with the results of elemental concentration mea-



Spectrum	Elemental composition, wt. %				
	Fe	Cr	Co	Ti	O
1	54.9	28.7	15.3	1.0	–
2	53.3	29.8	15.4	1.5	–
3	6.3	4.2	1.7	56.4	31.4
4	41.4	34.1	22.2	2.2	–
5	50.2	25.7	23.4	0.7	–
6	0.7	0.9	0.3	62.2	35.9

c

Fig. 2. SEM images of microsections of alloys Kh28K15T_P (a) and Kh32K22T_P (b) after sintering, and EDS analysis results at points 1–6 (c)

Рис. 2. РЭМ-фотографии микрошлифов сплавов X28K15T_П (a) и X32K22T_П (b) после спекания и результаты ЭДС-анализа в точках 1–6 (c)

surements obtained by EDS for different structural constituents.

According to the obtained diffraction patterns (Fig. 1), the phase composition of the Fe–28Cr–15Co and Fe–32Cr–22Co alloys differs significantly immediately after sintering. The structure of the Kh28K15T_H and Kh28K15T_P samples consists of a BCC α -phase solid solution and inclusions of the tetragonal σ -phase. In the microstructure image of the Kh28K15T_P alloy (Fig. 2, *a*), the σ -phase inclusions appear as white bands within the gray α -phase matrix, mainly located along grain boundaries. This is consistent with numerous studies indicating that σ -phase inclusions typically form at grain boundaries. The elemental composition of the phases is relatively similar, although the σ -phase inclusions exhibit a slightly elevated chromium concentration.

The structures of the Kh32K22T_H and Kh32K22T_P alloys consist of a σ -phase solid solution and FCC γ -phase inclusions (Fig. 1). No traces of the α -phase are observed in these samples, which can be attributed to the polymorphic nature of the $\alpha \rightarrow \sigma$ transformation during cooling of Fe–Cr–Co alloys with elevated Cr and Co contents. It should be noted that the diffraction peaks in the patterns of Kh32K22T_H and Kh32K22T_P may also indicate the presence of two distinct σ -phases based on Fe–Cr and Co–Cr systems, which are compositionally similar, as well as two γ -phases. The peaks of these phases may partially or fully overlap, which complicates their identification.

In the microstructure image of the Kh32K22T_P alloy (Fig. 2, *b*), in contrast to Kh28K15T_P, the σ -phase-based matrix appears as the brightest structural component, while all inclusions are darker. According to the EDS data (Fig. 2, *c*), the inclusions show increased Fe content and reduced Cr content, which confirms the presence of the γ -phase in the sample. All oxide inclusions observed in pore regions in both alloys are titanium oxides.

X-ray diffraction patterns of the Fe–28Cr–15Co and Fe–32Cr–22Co alloys containing different titanium sources after heat treatment are shown in Fig. 3, and their microstructure images are presented in Fig. 4. The structure of all samples represents a BCC α -phase solid solution (Fig. 3). The spinodal decomposition into α_1 and α_2 phases that occurs during thermal treatment was not detected in the diffraction patterns due to peak broadening. In the patterns of Kh28K15T_H and Kh32K22T_H, diffraction peaks of a secondary phase are also present, which may correspond to iron or cobalt oxides. However, according to earlier EDS analysis and elemental mapping [30], all oxide inclusions in the structure are titanium oxides. In addition,

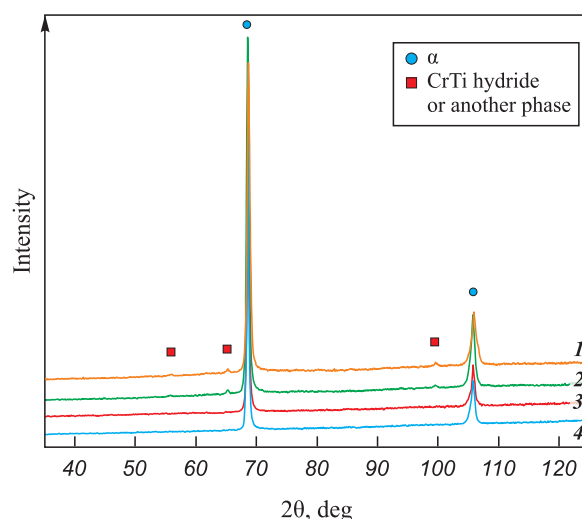


Fig. 3. X-ray diffraction patterns of Fe–Cr–Co alloys doped with titanium after heat treatment

1 – Kh32K22T_H, 2 – Kh28K15T_H, 3 – Kh32K22T_P, 4 – Kh28K15T_P

Рис. 3. Дифрактограммы сплавов системы Fe–Cr–Co с добавками титана после термической обработки

1 – X32K22T_Г, 2 – X28K15T_Г, 3 – X32K22T_П, 4 – X28K15T_П

among the main components of Fe–Cr–Co alloys, chromium is known to oxidize first.

Additional analysis indicated that the diffraction peaks of the secondary phase may also correspond to a hydride of a Ti–Cr-based intermetallic compound, which may partly account for the formation of the porous structure observed in the samples containing it (Fig. 4, *a, b*). However, the initial amount of titanium hydride in the system is small. Hydrides of Ti–Cr-based compounds are also characterized by low stability, so it cannot be conclusively identified which specific compound is responsible for the secondary phase peaks observed in the obtained alloys. Notably, these peaks may already be present in the diffraction patterns after sintering (see Fig. 1, *b*); however, at positions such as $2\theta = 66^\circ$ and 100° , they are overlapped by the σ -phase peaks, which further complicates their identification.

Microstructural analysis of the samples revealed noticeable differences in the porous structure depending on the titanium source. As seen in Fig. 4, *a, b*, the samples containing titanium hydride exhibit numerous elongated dark inclusions forming a branched porous network, indicative of incomplete sintering. This type of structure is considered intermediate and may have resulted from incomplete dehydrogenation of titanium during the sintering heating process. Rapid healing of open pores may have trapped hydrogen within the material, thereby impeding the removal of residual porosity and promoting the formation of elongated inclusions under internal pressure.

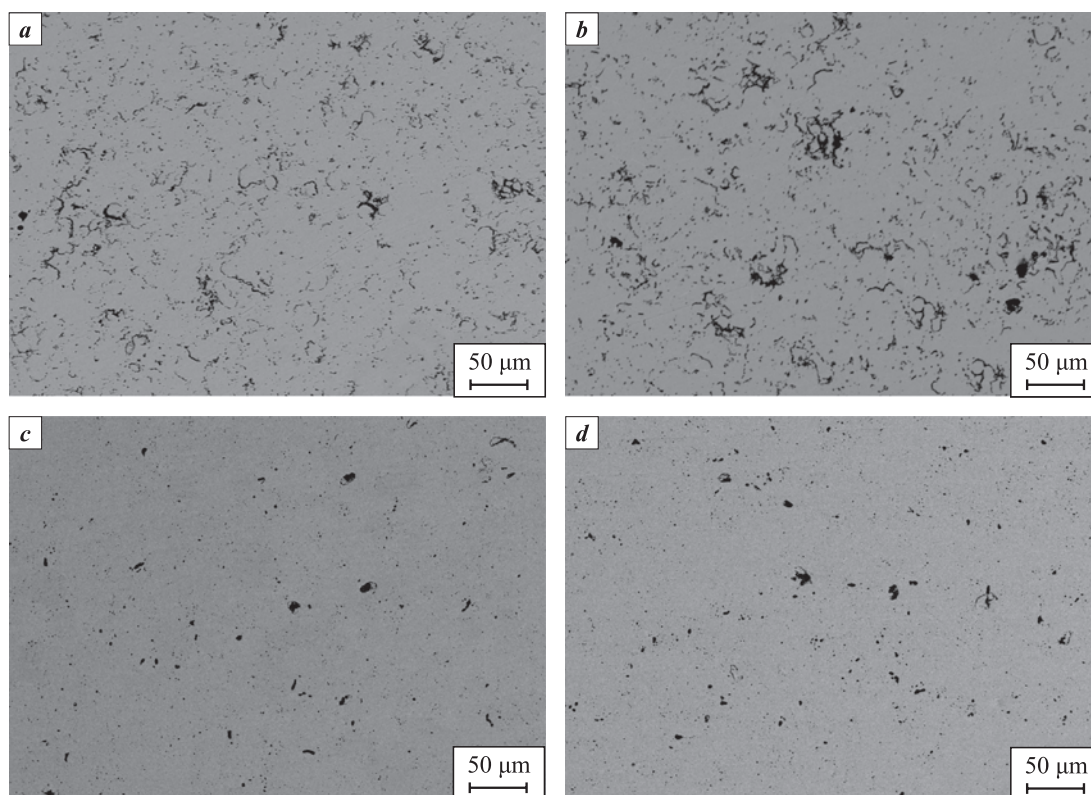


Fig. 4. SEM images of microsections of alloys Kh28K15T_H (a), Kh32K22T_H (b), Kh28K15T_P (c), and Kh32K22T_P (d) after heat treatment

Рис. 4. РЭМ-фотографии микрошлифов сплавов X28K15T_Г (a), X32K22T_Г (b), X28K15T_П (c) и X32K22T_П (d) после термической обработки

In the alloys with PTS-1 titanium powder, the pore structure is characterized by dark inclusions 5–10 μm in size, fairly uniformly distributed throughout the matrix, along with significantly smaller pores approximately 1–2 μm in size (Fig. 4, c, d). The alloys with titanium hydride (Fig. 4, a, b) exhibit a visibly higher number and volume of inclusions compared to those with titanium powder (Fig. 4, c, d), which correlates with the lower relative density values measured for these samples. In addition, the smaller inclusions in Fig. 4, c, d tend to cluster, suggesting incomplete pore closure during sintering.

The magnetic property analysis revealed significant differences in B_r , H_c , and $(BH)_{\text{max}}$ values depending on the titanium source. The heat treatment dependence of the magnetic properties is shown in Fig. 5. The use of titanium hydride led to increased maximum coercivity (H_c up to 41.1 and 57.2 kA/m for Kh28K15T_H and Kh32K22T_H, respectively) and reduced residual induction (B_r up to 0.8 and 0.79 T), compared to Kh28K15T_P and Kh32K22T_P alloys (up to 0.84 and 0.82 T, respectively). The lower B_r values are mainly attributed to increased porosity in the samples with titanium hydride.

The temperature dependence of residual induction (Fig. 5, a, b) is nearly identical for all alloys: as t_1 increases, Br values decrease monotonically, similar to the behavior observed in many other isotropic Fe–Cr–Co alloys. The observed increase in coercivity is likely associated with a higher density of defects and internal stresses in the structure due to incomplete titanium dehydrogenation. The temperature dependence of H_c for all alloys exhibits a maximum at $t_1 \sim 645\text{--}650^\circ\text{C}$ (Fig. 5, c, d). For both H_c and B_r , even a 5 $^\circ\text{C}$ change in t_1 can have a pronounced effect on their values, highlighting the sensitivity of spinodal decomposition and the final magnetic properties of the alloys to the processing conditions. The $(BH)_{\text{max}}$ curves (Fig. 5, e, f) for alloys with different titanium sources are relatively similar, as the improvement in one magnetic parameter is offset by the decline in another. The highest values of $(BH)_{\text{max}}$ reached 11.0–11.5 kJ/m³ for both Kh28K15T_H and Kh28K15T_P, and 14.0–14.5 kJ/m³ for Kh32K22T_H and Kh32K22T_P.

A comparison of the mechanical properties of the investigated Fe–Cr–Co alloys containing different titanium sources was carried out. The samples with the best set of magnetic properties were subjected to compression testing. The experimental stress–strain curves are

shown in Fig. 6, and the results of mechanical property evaluation are presented in Table 2. The tests were conducted up to a strain of 25 % (ϵ).

Analysis of the stress–strain curves (Fig. 6) shows that all the titanium-doped alloys investigated in this study exhibit good ductility. With the exception of Kh32K22T_P, all other samples underwent deformation up to a strain of 25 % without fracture. An increase in chromium and cobalt content in the alloys resulted in a rise in yield strength ($\sigma_{0.2}$) from 1000 to 1200–1400 MPa (Table 2). At the same time, the stress–strain curves of the alloys with different

Table 2. Results of yield strength $\sigma_{0.2}$, compressive strength σ_c , and fracture strain ϵ_f measurements for the investigated alloys containing different titanium sources

Таблица 2. Результаты определения предела текучести ($\sigma_{0.2}$), прочности на сжатие (σ_c) и деформации при разрушении (ϵ_f) исследуемых сплавов, содержащих разные источники титана

Alloy	$\sigma_{0.2}$, MPa	σ_c , MPa	ϵ_f (100 %)
Kh28K15T_H	990 ± 30	>1580	>25.0
Kh28K15T_P	1000 ± 30	>1650	>25.0
Kh32K22T_H	1400 ± 40	>1850	>25.0
Kh32K22T_P	1240 ± 30	1850 ± 10	23.6

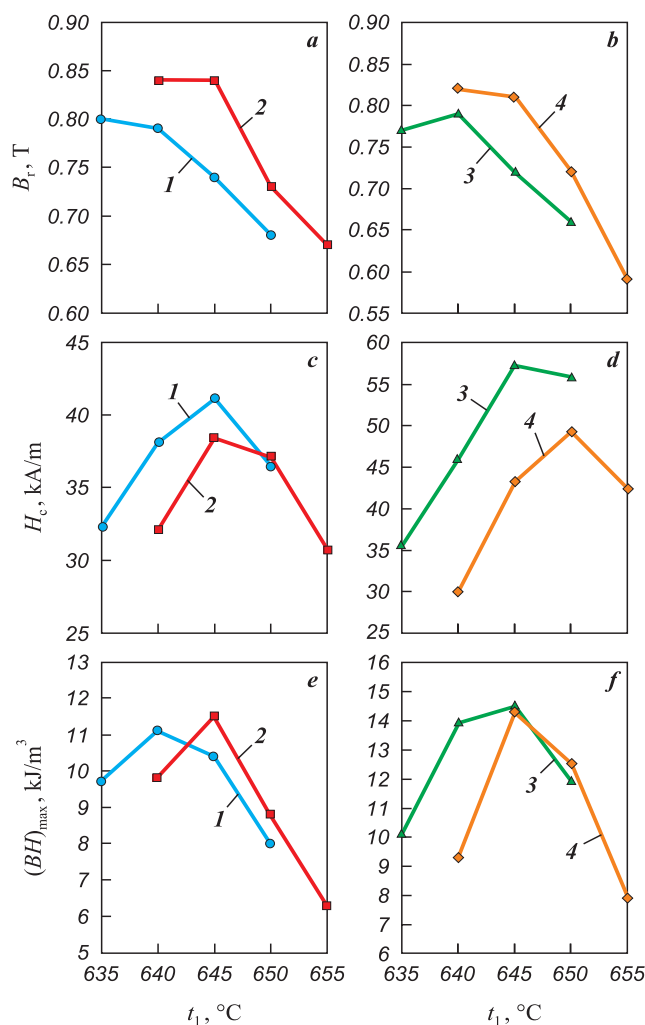


Fig. 5. Dependencies of residual induction (a, b), coercivity (c, d), and maximum energy product (e, f) on the heat treatment t_1 for the investigated Fe–Cr–Co alloys containing different titanium sources

1 – Kh28K15T_H, 2 – Kh28K15T_P, 3 – Kh32K22T_H, 4 – Kh32K22T_P

Рис. 5. Зависимости остаточной индукции (a, b), коэрцитивной силы (c, d) и максимального энергетического произведения (e, f) от температуры термообработки (t_1) исследуемых сплавов системы Fe–Cr–Co, содержащих разные источники титана

1 – X28K15T_Г, 2 – X28K15T_П, 3 – X32K22T_Г, 4 – X32K22T_П

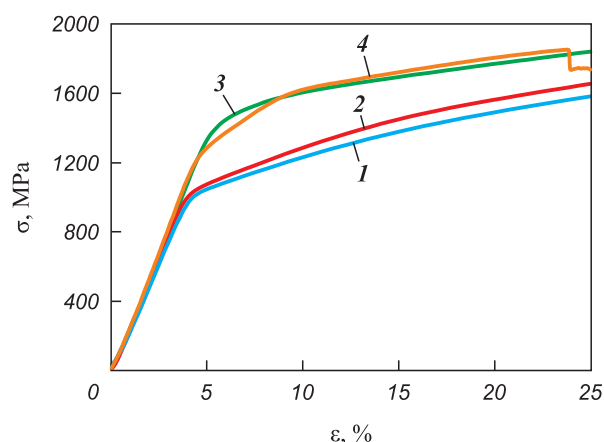


Fig. 6. Stress–strain curves of the investigated Fe–Cr–Co alloy samples containing different titanium sources

1 – Kh28K15T_H, 2 – Kh28K15T_P, 3 – Kh32K22T_H, 4 – Kh32K22T_P

Рис. 6. Кривые деформирования образцов исследуемых сплавов системы Fe–Cr–Co, содержащих разные источники титана

1 – X28K15T_Г, 2 – X28K15T_П, 3 – X32K22T_Г, 4 – X32K22T_П

titanium sources show only minor differences, despite noticeable variations in porosity and magnetic properties (Fig. 6).

Conclusions

Based on the results of this study on powder-processed hard magnetic Fe–Cr–Co alloys doped with titanium from different sources, the following conclusions can be drawn.

1. Doping with titanium hydride powder leads to an increase in residual porosity from 2 to 4 %. Phase composition analysis revealed the presence of a secondary phase, most likely a hydride of a Ti–Cr-based intermetallic compound. Microstructural analysis showed that the pore structure in the alloys containing titanium hydride is branched, which is typical of incomplete sin-

tering. This suggests that the increased porosity is primarily due to incomplete dehydrogenation of titanium hydride during the heating stage of sintering.

2. Magnetic property measurements demonstrated that samples doped with PTS-1 titanium powder exhibited higher residual induction values (B_r up to 0.84 T) compared to those doped with titanium hydride, which is attributed to lower residual porosity. Conversely, the titanium hydride-doped samples showed higher coercivity values (H_c up to 57.2 kA/m).

3. Compression tests showed that, despite differences in density and magnetic properties, the stress-strain curves of alloys with different titanium sources were nearly identical. The Fe–32Cr–22Co–2Ti samples exhibited higher yield strength ($\sigma_{0.2} = 1200\div 1400$ MPa) compared to the Fe–28Cr–15Co–2Ti samples ($\sigma_{0.2} = 1000$ MPa). All titanium-doped alloys investigated in this study showed good ductility, with most of them deforming up to 25 % strain without fracturing.

References / Список литературы

1. Kaneko H., Homma M., Minowa T. Effect of V and V+Ti additions on the structure and properties of Fe–Cr–Co ductile magnet alloys. *IEEE Transactions on Magnetics*. 1976;12(6):977–979.
<https://doi.org/10.1109/TMAG.1976.1059239>
2. Tao S., Ahmad Z., Zhang P., Zheng X., Wang F., Xu X. Enhancement of magnetic and microstructural properties in Fe–Cr–Co–Mo–V–Zr–Y permanent magnetic alloy. *Journal of Magnetism and Magnetic Materials*. 2019;484: 88–94. <https://doi.org/10.1016/j.jmmm.2019.04.004>
3. Perminov A.S., Maslennikov S.O., Lileev A.S., Shuvaeva E.A., Stolyarov V.L., Zhukov D.G. Concentration distribution of elements and variation in phase composition during solid-solution decomposition in Fe–Cr–Co alloy. *Steel in Translation*. 2010; 40(3):216–218.
<https://doi.org/10.3103/S0967091210030058>
Перминов А.С., Масленников С.О., Лилеев А.С., Шуваяева Е.А., Столяров В.Л., Жуков Д.Г. Моделирование пространственного распределения концентраций элементов и кинетики изменения количества фаз при распаде твердого раствора в сплаве Fe–Cr–Co. *Известия вузов. Черная металлургия*. 2010;53(3):32–34.
4. Belozеров E.V., Mushnikov N.V., Ivanova G.V., Shchegoleva N.N., Serikov V.V., Kleinerman N.M., Vershinin A.V., Uimin M.A. High-strength magnetically hard Fe–Cr–Co-based alloys with reduced content of chromium and cobalt. *The Physics of Metals and Metallography*. 2012;113(4):319–325.
<https://doi.org/10.1134/S0031918X12040023>
Белозеров Е.В., Мушников Н.В., Иванова Г.В., Щеголева Н.Н., Сериков В.В., Клейнерман Н.М., Вершинин А.В., Уймин М.А. Высокопрочные магнитотвердые сплавы на основе Fe–Cr–Co с пониженным содержанием хрома и кобальта. *Физика металлов и металлургия*. 2012;113(4):339–346.
5. Korneva A., Korznikova G., Berent K., Korznikov A., Kashaev R., Bogucka J., Sztwiertnia K. Microstructure evolution and magnetic properties of hard magnetic FeCr22Co15 alloy subjected to tension combined with torsion. *Journal of Alloys and Compounds*. 2014;615(S1):S300–S303.
<https://doi.org/10.1016/j.jallcom.2014.01.207>
6. Han X.H., Bu S.J., Wu X., Sun J.B., Zhang Y., Cui C.X. Effects of multi-stage aging on the microstructure, domain structure and magnetic properties of Fe–24Cr–12Co–1.5Si ribbon magnets. *Journal of Alloys and Compounds*. 2017; 694:103–110.
<https://doi.org/10.1016/j.jallcom.2016.09.316>
7. Xiang Z., Zhang L., Xin Y., An B., Niu R., Mardani M., Siegrist T., Lu J., Goddard R.E., Man T., Wang E., Han K. Ultrafine microstructure and hardness in Fe–Cr–Co alloy induced by spinodal decomposition under magnetic field. *Materials and Design*. 2021;199:109383.
<https://doi.org/10.1016/j.matdes.2020.109383>
8. Gao Q., Gong M., Wang Y., Qu F., Huang J. Phase transformation and properties of Fe–Cr–Co alloys with low cobalt content. *Materials Transactions*. 2015;56(9):1491–1495.
<https://doi.org/10.2320/matertrans.M2015077>
9. Efremov D.V., Gerasimova A.A. Production of Fe–Cr–Co-based magnets by selective laser sintering. *Steel in Translation*. 2021;51(10):688–692.
<https://doi.org/10.3103/S0967091221100028>
Ефремов Д.В., Герасимова А.А. Получение магнитов из материала системы Fe–Cr–Co методами селективного лазерного спекания. *Известия вузов. Черная металлургия*. 2021;64(10):721–727.
<https://doi.org/10.17073/0368-0797-2021-10-721-727>
10. Marieva M.A., Shatsov A.A. Prediction of the concentration inhomogeneity of powder magnetic hard alloys based on the Fe–Cr–Co–Mo system and the effect of Sm additions on their magnetic properties. *Powder Metallurgy and Functional Coatings*. 2023;17(1):12–20.
<https://doi.org/10.17073/1997-308X-2023-1-12-20>
Мариева М.А., Шацов А.А. Прогнозирование концентрации неоднородности порошковых магнитотвердых сплавов на основе системы Fe–Cr–Co–Mo и влияние добавок Sm на их магнитные свойства. *Известия вузов. Порошковая металлургия и функциональные покрытия*. 2023;17(1):12–20
<https://doi.org/10.17073/1997-308X-2023-1-12-20>
11. Ustyukhin A.S., Ankudinov A.B., Zelensky V.A., Alymov M.I., Milyaev I.M., Vompe T.A. Synthesis, thermal treatment, and characterization of sintered hard magnetic Fe–30Cr–16Co alloy. *Journal of Alloys and Compounds*. 2022;902:163754.
<https://doi.org/10.1016/j.jallcom.2022.163754>
12. Zhukov A.S., Kuznetsov P.A., Kamynin A.V., Gavrikov I.S., Barakhtin B.K. Multifractal analysis and magnetic properties of magnetically hard Fe–Cr–Co alloy produced by selective laser melting. *Russian Engineering Research*. 2021;41(4):325–328.
<https://doi.org/10.3103/S1068798X21040250>
13. He Y., Zhang H., Su H., Shen P., Hou Y., Zhou D. In situ alloying of Fe–Cr–Co permanent magnet by selective laser melting of elemental iron, chromium and cobalt mixed

- powders. *Metals*. 2022;12(10):1634.
<https://doi.org/10.3390/met12101634>
14. Mairhofer T., Arneitz S., Hofer F., Sommitsch C., Kothleitner G. Micro- and nanostructure of additively manufactured, in-situ alloyed, magnetic spinodal Fe₅₄Cr₃₁Co₁₅. *Journal of Materials Science*. 2023;58:7119–7135.
<https://doi.org/10.1007/s10853-023-08445-z>
 15. Generalova K.N., Ryaposov I.V., Shatsov A.A. Effect of Mo and W additions on the magnetic hysteresis properties of a powder ridge alloy. *Metal Science and Heat Treatment*. 2020;61:657–662.
<https://doi.org/10.1007/s11041-020-00474-8>
 Генералова К.Н., Ряпосов И.В., Шацов А.А. Влияние добавок Мо и W на гистерезисные магнитные свойства порошкового гребневого сплава. *Металловедение и термическая обработка металлов*. 2019;(10):72–77.
<https://doi.org/10.30906/mitom.2019.10.72-77>
 16. Amini Rastabi R., Ghasemi A., Tavooosi M., Ramazani M. Magnetic features of Fe–Cr–Co alloys with tailoring chromium content fabricated by spark plasma sintering. *Journal of Magnetism and Magnetic Materials*. 2017;426:744–752. <https://doi.org/10.1016/j.jmmm.2016.10.132>
 17. He Y., Hou Y., Shen P., Zhang H., Zhou D., Su H. Fabricating functionally graded Fe–Cr–Co permanent magnetic alloys via laser powder bed fusion. *Journal of Iron and Steel Research International*. 2024;31:729–737.
<https://doi.org/10.1007/s42243-023-01088-z>
 18. Ajia S., Asa H., Toyoda Y., Sato M., Matsuura M., Tezuka N., Sugimoto S. Development of an alternative approach for electromagnetic wave absorbers using Fe–Cr–Co alloy powders. *Journal of Alloys and Compounds*. 2022;903:163920.
<https://doi.org/10.1016/j.jallcom.2022.163920>
 19. Liu J.T., Xu X.L., Feng G.N., Yang X.Y., Zhao D., Zuo M.G., Liu C.Y., Feng C., Liu S., Li B.H., Yu G.H. Coercivity modulation of FeCoCrMoTi films by artificial magnetic phase defects engineering based on multilayer structure. *Acta Materialia*. 2023;259:119241.
<https://doi.org/10.1016/j.actamat.2023.119241>
 20. Zhao D., Xu X.L., Cao Y., Zhai M.Y., Lu S., Kang P., Liu J.T., Yang X.Y., Zuo M.G., Liu C.Y., Hu W.Y., Ma X.J., Yu G.H. Improving magnetic properties of FeCrCo films by facilitating the internal α - γ phase transition through Pt diffusion. *Acta Materialia*. 2025;282:120469.
<https://doi.org/10.1016/j.actamat.2024.120469>
 21. Perminov A.S., Maslennikov S.O., Lileev A.S., Shuvaeva E.A., Vvedenskii V.Y. Isothermal decomposition in Fe–Cr–Co alloy. *Steel in Translation*. 2009;39(9):755–756.
<https://doi.org/10.3103/S0967091209090083>
 Перминов А.С., Масленников С.О., Лилеев А.С., Шуваяева Е.А., Введенский В.Ю. Моделирование изотермического распада в сплаве Fe–Cr–Co. *Известия вузов. Черная металлургия*. 2009;52(9):55–56.
 22. Zhang L., Xiang Z., Li X., Wang E. Spinodal decomposition in Fe–25Cr–12Co alloys under the influence of high magnetic field and the effect of grain boundary. *Nanomaterials*. 2018;8(8):578.
<https://doi.org/10.3390/nano8080578>
 23. Iwaizako H., Okugawa M., Saito K., Koizumi Y., Chiba A., Tachiya Y., Ohnuma M., Kuritani K. Spinodal decomposition in plastically deformed Fe–Cr–Co magnet alloy. *ISIJ International*. 2022;62(6):1268–1274.
<https://doi.org/10.2355/isijinternational.ISIJINT-2021-441>
 24. Kozvonin V.A., Shatsov A.A., Ryaposov I.V., Generalova K.N., Spivak L.V. Phase transformations and properties of concentration-inhomogeneous magnetic materials based on the Fe–30%Cr–27%Co system. *Powder Metallurgy and Functional Coatings*. 2019;13(1):82–90. (In Russ.).
<https://doi.org/10.17073/1997-308X-2019-1-82-90>
 Козвонин В.А., Шацов А.А., Ряпосов И.В., Генералова К.Н., Спивак Л.В. Фазовые превращения и свойства концентрационно-неоднородных магнитных материалов на основе системы Fe–30%Cr–27%Co. *Известия вузов. Порошковая металлургия и функциональные покрытия*. 2019;13(1):82–90.
<https://doi.org/10.17073/1997-308X-2019-1-82-90>
 25. Ahmad Z., ul Haq A., Yan M., Iqbal Z. Evolution of phase, texture, microstructure and magnetic properties of Fe–Cr–Co–Mo–Ti permanent magnets. *Journal of Magnetism and Magnetic Materials*. 2012;324:2355–2359.
<https://doi.org/10.1016/j.jmmm.2012.02.040>
 26. Tao S., Ahmad Z., Zhang P., Zheng X., Zhang S. Effects of Sm on structural, textural and magnetic properties of Fe–28Cr–20Co–3Mo–2V–2Ti hard magnetic alloy. *Journal of Alloys and Compounds*. 2020;816:152619.
<https://doi.org/10.1016/j.jallcom.2019.152619>
 27. Ustyukhin A.S., Zelenskii V.A., Milyaev I.M., Shustov V.S., Yusupov V.S. Studies of properties of isotropic hard magnetic powder alloys Fe–30Cr–20Co–2Mo (Kh30K20M2) doped with niobium. *Steel in Translation*. 2022;52(10):996–1002.
<https://doi.org/10.3103/S096709122210014X>
 28. Belyukova M.A., Shatsov A.A. Phase transformations, microstructure formation, and magnetic properties of a hysteresis alloy based on the Fe–Cr–Co–Mo system doped with Sm, Zr, and Cu. *Powder Metallurgy and Functional Coatings*. 2024;18(4):35–44.
<https://doi.org/10.17073/1997-308X-2024-4-35-44>
 Бельтюкова М.А., Шацов А.А. Особенности фазовых превращений, формирования микроструктуры и магнитных свойств гистерезисного сплава на основе системы Fe–Cr–Co–Mo, легированного Sm, Zr и Cu. *Известия вузов. Порошковая металлургия и функциональные покрытия*. 2024;18(4):35–44.
<https://doi.org/10.17073/1997-308X-2024-4-35-44>
 29. Ustyukhin A.S., Zelensky V.A., Milyaev I.M., Alymov M.I., Ashmarin A.A., Ankudinov A.B., Sergienko K.V. Synthesis and magnetic hysteresis properties of an aluminum-doped isotropic hard-magnetic Fe–Cr–Co powder alloy. *Inorganic Materials: Applied Research*. 2024;15(2):480–488.
<https://doi.org/10.1134/S2075113324020424>
 30. Ustyukhin A.S., Zelensky V.A., Milyaev I.M., Shustov V.S., Shibakova N.S. Influence of individual dopants on density and magnetic properties of isotropic hard magnetic Fe–28Cr–15Co alloy. *Stal*. 2025;1:45–51. (In Russ.).
 Устюхин А.С., Зеленский В.А., Милеев И.М., Шустов В.С., Шибакова Н.С. Влияние индивидуальных легирующих добавок на плотность и магнитные свойства изотропного магнитотвердого сплава Fe–28Cr–15Co. *Сталь*. 2025;1:45–51.

Information about the Authors




Сведения об авторах

Aleksei S. Ustyukhin – Cand. Sci. (Eng.), Junior Research Scientist at the Laboratory of Physical Chemistry of Surfaces and Ultrafine Powder Materials, A.A. Baikov Institute of Metallurgy and Materials Science of the Russian Academy of Sciences Russian Federation (IMET RAS)

 **ORCID:** 0000-0003-1578-4883


 **E-mail:** fcbneo@yandex.ru

Viktor A. Zelensky – Cand. Sci. (Phys.-Math.), Leading Researcher at the Laboratory of Physical Chemistry of Surfaces and Ultrafine Powder Materials, IMET RAS

 **ORCID:** 0000-0002-4441-9132


 **E-mail:** zelensky55@bk.ru

Igor M. Milyaev – Dr. Sci. (Eng.), Leading Researcher at the Laboratory of Plastic Deformation of Metallic Materials, IMET RAS

 **ORCID:** 0000-0002-0591-2645

 **E-mail:** imilyaev@mail.ru

Dmitry Yu. Kovalev – Dr. Sci. (Phys.-Math.), Head of the Laboratory of X-Ray Investigation, Merzhanov Institute of Structural Macrokinetic and Materials Science Russian Academy of Sciences (ISMAN)

 **ORCID:** 0000-0002-8285-5656


 **E-mail:** kovalev@ism.ac.ru

Vadim S. Shustov – Cand. Sci. (Eng.), Senior Research Scientist at the Laboratory of Physical Chemistry of Surfaces and Ultrafine Powder Materials, IMET RAS

 **ORCID:** 0000-0001-6395-3747

 **E-mail:** vshscience@mail.ru

Mikhail I. Alymov – Dr. Sci. (Eng.), Corresponding Member of RAS, Director of ISMAN, Head of the Laboratory of Physical Chemistry of Surfaces and Ultrafine Powder Materials, IMET RAS

 **ORCID:** 0000-0001-6147-5753


 **E-mail:** mialymov@mail.ru

Алексей Сергеевич Устюхин – к.т.н., мл. науч. сотрудник лаборатории физикохимии поверхности и ультрадисперсных порошковых материалов Института металлургии и материаловедения им. А.А. Байкова Российской академии наук (ИМЕТ РАН)

 **ORCID:** 0000-0003-1578-4883

 **E-mail:** fcbneo@yandex.ru

Виктор Александрович Зеленский – к.ф.-м.н., вед. науч. сотрудник лаборатории физикохимии поверхности и ультрадисперсных порошковых материалов ИМЕТ РАН

 **ORCID:** 0000-0002-4441-9132


 **E-mail:** zelensky55@bk.ru

Игорь Матвеевич Миляев – д.т.н., вед. науч. сотрудник лаборатории пластической деформации металлических материалов ИМЕТ РАН

 **ORCID:** 0000-0002-0591-2645


 **E-mail:** imilyaev@mail.ru

Дмитрий Юрьевич Ковалев – д.ф.-м.н., зав. лабораторией рентгеноструктурных исследований Института структурной макрокинетики и проблем материаловедения им. А.Г. Мерзханова Российской академии наук (ИСМАН)

 **ORCID:** 0000-0002-8285-5656

 **E-mail:** kovalev@ism.ac.ru

Вадим Сергеевич Шустов – к.т.н., науч. сотрудник лаборатории физикохимии поверхности и ультрадисперсных порошковых материалов ИМЕТ РАН

 **ORCID:** 0000-0001-6395-3747

 **E-mail:** vshscience@mail.ru

Михаил Иванович Алымов – д.т.н., чл.кор. РАН, директор ИСМАН, зав. лабораторией физикохимии поверхности и ультрадисперсных порошковых материалов ИМЕТ РАН

 **ORCID:** 0000-0001-6147-5753

 **E-mail:** mialymov@mail.ru

Contribution of the Authors



Вклад авторов

A. S. Ustyukhin – defined the research objectives, performed electron microscopy analysis of the structure, participated in discussion of results, and wrote the manuscript.

V. A. Zelensky – research objectives, conducted powder mixing, pressing, sintering, and quenching of the samples, participated in the discussion of the results, and contributed to manuscript editing.

I. M. Milyaev – carried out heat treatment and magnetic property measurements.

D. Yu. Kovalev – performed X-ray phase analysis and participated in discussion of results.

V. S. Shustov – measured the density, prepared samples for compression testing, and participated in discussion of results.

M. I. Alymov – defined the research objectives and participated in discussion of results.

А. С. Устюхин – определение цели работы, проведение исследований структуры электронной микроскопией, участие в обсуждении результатов, написание текста статьи.

В. А. Зеленский – определение цели работы, подготовка смесей, прессование, спекание и закалка образцов, участие в обсуждении результатов и редактировании статьи.

И. М. Миляев – термическая обработка и измерение магнитных свойств образцов.

Д. Ю. Ковалев – рентгенофазовый анализ образцов и обсуждение результатов.

В. С. Шустов – измерение плотности, подготовка образцов для механических испытаний на сжатие, участие в обсуждении результатов.

М. И. Алымов – определение цели работы, участие в обсуждении результатов.

Received 28.02.2025

Revised 19.03.2025

Accepted 24.03.2025

Статья поступила 28.02.2025 г.

Доработана 19.03.2025 г.

Принята к публикации 24.03.2025 г.